Supporting Information

In situ integration of cocatalyst and heterojunction to WO_3 photoanode via phosphatization and protonation

Faqi Zhan [a,b,*], Haiyan Zhao [b], Guochang Wen [b], Zhiqing Ma [a], Yisi Liu [c], Min Zhu [b], Yuehong Zheng [b], Dalin Chen [a,*], Peiqing La [b]

[a] State Key Laboratory of Nickel and Cobalt Resources Comprehensive Utilization, Jinchang, 737100, China

[b] State Key Laboratory of Advanced Processing and Recycling of Non-Ferrous Metals, Lanzhou University of Technology, Lanzhou 730050, China

[c] Institute of Advanced Materials, Hubei Normal University, Huangshi, 415000, China

[*]Corresponding author. Tel.: +86 15209310025.

E-mail address: zhanfaqi@lut.edu.cn (Faqi Zhan), jnmcdalin@126.com (Dalin Chen).

Experimental section

Preparation of photoanodes films

WO_3 films: The WO_3 plate-like arrays film was prepared according to previous literature method of our group.[1] In the typical hydrothermal synthesis process, 0.23 g Na_2WO_4•$2H_2O$ was used as the tungsten source and dissolved in 30 mL of deionized water under continuous stirring at room temperature. Then, 6 mL of 3 M HCl was added drop by drop to form a white precipitate, followed by the addition of 0.20 g $(NH_4)_2C_2O_4$ into the above suspension, which was used as structure-directing agent. After 20 minutes of stirring, the suspension became transparent and then about 34 mL of deionized water was added into it with additional stirring for 30 min. Before the as-prepared precursor was transferred into a Teflon-lined stainless autoclave (100 mL volume), the FTO glass substrates cleaned ultrasonically by acetone, isopropanol, methanol, and deionized water in sequence and finally dried in a nitrogen stream, were placed and leaned against the wall of the Teflon-vessel with the conducting side facing down. After the autoclave was sealed, the hydrothermal synthesis process was carried out at 120 ^oC for 12 h. After the autoclave was allowed to cool down to room temperature naturally, the films were taken out and rinsed with absolute ethanol several times and dried at 60 ^oC for 30 min.

$NiWO_4/WO_3$ film: The $NiWO_4/WO_3$ film was prepared according to previous literature method of our group.[2] A chemical-bath in-situ deposition method was used to synthesize the $NiWO_4$ nanoparticles on the surface of as-prepared WO_3 plate-like arrays films. In this method, 50 mM $Ni(CH_3COO)_2$ in ethanol solution were prepared as the nickel source. Then the WO_3 films were vertically dipped into above solution for 1 h, followed by washing with ethanol and drying at 60 ^oC to remove the ethanol. Finally, the as-prepared films were calcined at 500 ^oC for 1 h.

$NiP_x/NiWO_4/WO_3$ film: The as-prepared $NiWO_4/WO_3$ film and 0.5 g of $NaH_2PO_2 \cdot H_2O$ were put at two separate positions in a ceramic boat inside a tube furnace with $NaH_2PO_2 \cdot H_2O$ at the upstream of the gas flow. After flushed with argon (Ar), the center of the furnace was elevated to 300 °C at a ramping rate of 2 °C min^{-1} and kept at this temperature for 0.5 h in a static Ar atmosphere, and then naturally cooled down to ambient temperature. The $H_{0.33}WO_3$ film was obtained by using the WO_3 film as the base materials through phosphatization process.

Characterization

The microscopic morphologies were examined by field-emission scanning electron microscope (FESEM, Nova NanoSEM 230) and high resolution transmission electron microscope (HRTEM, G2 F20). The surface chemical compositions and states of the films were detected by X-ray photoelectron spectroscopy (XPS, ESCALAB 250 XPS system). The crystal structures of all films were analysed by X-ray diffraction (XRD, D/Max2250, Rigaku Corporation, Japan) with Cu Kα (λ=0.15406 nm) radiation, and the UV-vis spectra were recorded by a diffused reflectance spectrophotometer with an integrating sphere (DR-UVS, Shimadzu 2450 spectrophotometer).

Photoelectrochemical measurements

Photoelectrochemical (PEC) performances of the as-prepared films were investigated using an electrochemical analyzer (Zennium, Zahner) in a standard three-electrode system with the samples as the working electrode, Pt plate as the counter electrode and an Ag/AgCl electrode as the reference electrode. A solution of 0.2 M Na_2SO_4 (pH=7) was used as the electrolyte. Simulated 1 sun light irradiation condition (100 mW/cm^2) was provided by a 500 W Xenon lamp with AM 1.5 G filters. All photoelectrodes were illuminated from the backside. The scan rate of the photocurrent-potential curve (J-V) was 20 mV/s. The incident photon-to-current conversion efficiency (IPCE) was measured using a Xenon lamp (150 W, Oriel) equipped with a monochromator at 1.0 V (*vs*. Ag/AgCl).

The measured potentials vs. Ag/AgCl were converted to the reversible hydrogen electrode (RHE) scale according to the Nernst equation: [3]

$$E_{RHE} = E_{Ag/AgCl} + 0.059\,pH + E^{\Theta}{}_{Ag/AgCl} \quad (1)$$

Where E_{RHE} is the converted potential vs. RHE, $E^{\Theta}{}_{\mathrm{Ag/AgCl}}$=0.1976 V at 25 ℃, and $E_{\mathrm{Ag/AgCl}}$ is the experimentally measured potential against an Ag/AgCl reference. The photoelectrochemical measurements were carried out in 0.2 M Na_2SO_4 (pH=7) at room temperature; therefore,

$$E_{RHE} = E_{Ag/AgCl} + 0.6\mathrm{V} \quad (2)$$

DFT calculations

The calculations in this study were performed using the CASTEP module based on density functional theory (DFT). The generalized gradient approximation (GGA) of Perdew-Burke-Ernzerh (PBE) was applied for the exchange-correlation function. Ionic

relaxations were performed until the atomic forces were converged to 0.03 eVÅ^{-1} by the Broyden-Fletcher-Goldfarb-Shanno (BFGS) optimization algorithm implemented in Atomic Simulation Environment (ASE). The convergence threshold for self-consistent-field (SCF) tolerance was set at 10^{-6} eV. For geometry and cell optimization, an 4×4×4 k-point mesh and a cutoff energy of 650 eV were applied for the primitive WO_3 and NiP_x unit cell. The core electrons were described by OTFG ultra-soft pseudopotentials During the geometry optimization, all atoms could relax except for the bottom layer of WO_3 (001) and NiP_x (110).

Figure Captions

Figure S1. The SEM images of as-prepared films: (a,b) WO_3, (c,d) $NiWO_4/WO_3$, (e,f) $NiP_x/NiWO_4/WO_3$ and (g) EDS spectrum of $NiP_x/NiWO_4/WO_3$ film.

Figure S2. The elemental-mapping distribution of $NiP_x/NiWO_4/WO_3$ film.

Figure S3. XPS spectra for W (a), O (b), Ni (c) and P (d) of $NiP_x/NiWO_4/WO_3$ film.

Figure S4. The photo absorbance spectrum of as-prepared films.

Figure S5. The I-t curves of WO_3 and $NiP_x/NiWO_4/WO_3$ films.

Figure S6. The dark current density of WO_3 and $NiP_x/NiWO_4/WO_3$ films.

Figure S7. Photo flux and theoretical maximum photocurrent of WO_3 film.

Figure S8. The Gibbs free energies and overpotentials (η) of different species adsorbed on WO_3 and NiP_2 surfaces.

Table S1 Comparison of literature with the similar catalyst system.

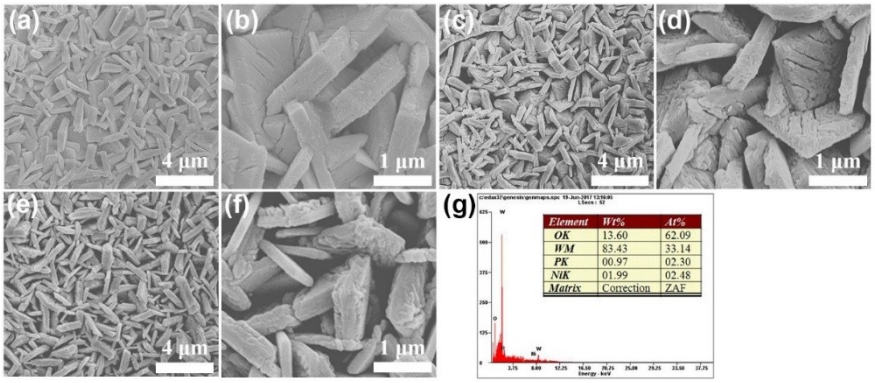

Figure S1. The SEM images of as-prepared films: (a,b) WO_3, (c,d) $NiWO_4/WO_3$, (e,f) $NiP_x/NiWO_4/WO_3$ and (g) EDS spectrum of $NiP_x/NiWO_4/WO_3$ film.

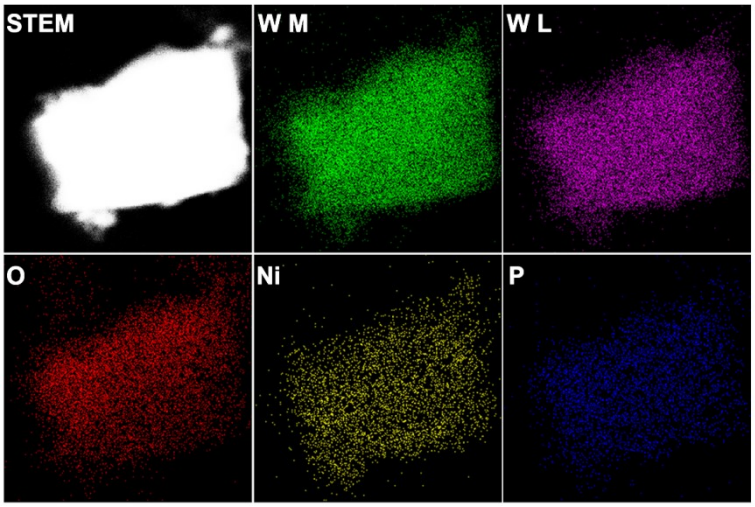

Figure S2. The elemental-mapping distribution of $NiP_x/NiWO_4/WO_3$ film.

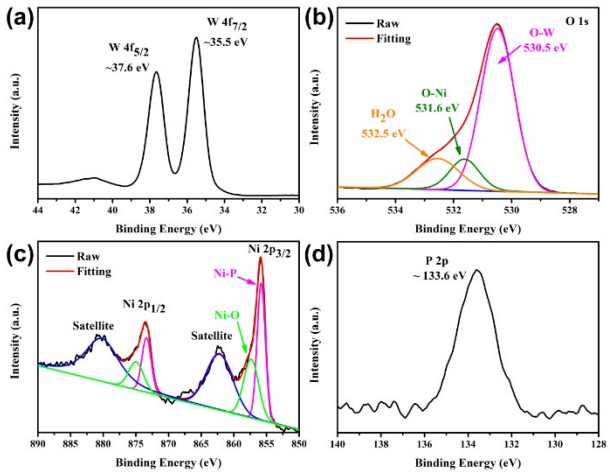

Figure S3. XPS spectra for W (a), O (b), Ni (c) and P (d) of $NiP_x/NiWO_4/WO_3$ film.

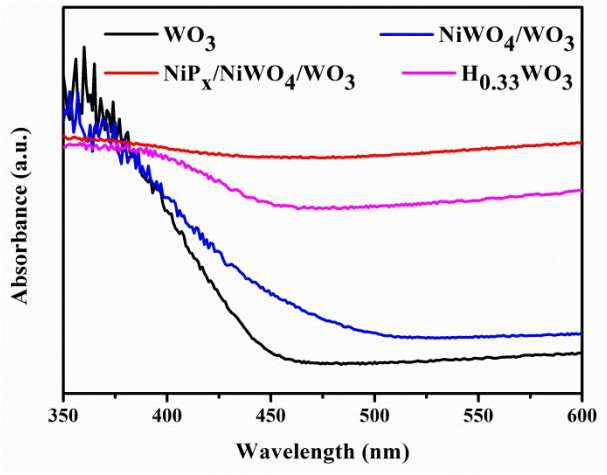

Figure S4. The photo absorbance spectrum of as-prepared films.

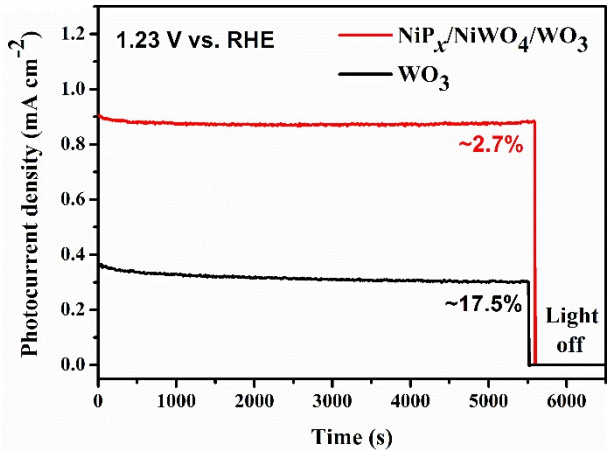

Figure S5. The I-t curves of WO_3 and $NiP_x/NiWO_4/WO_3$ films.

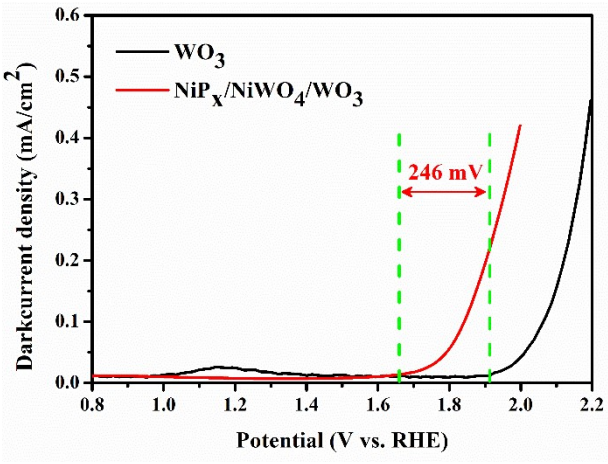

Figure S6. The dark current density of WO_3 and $NiP_x/NiWO_4/WO_3$ films.

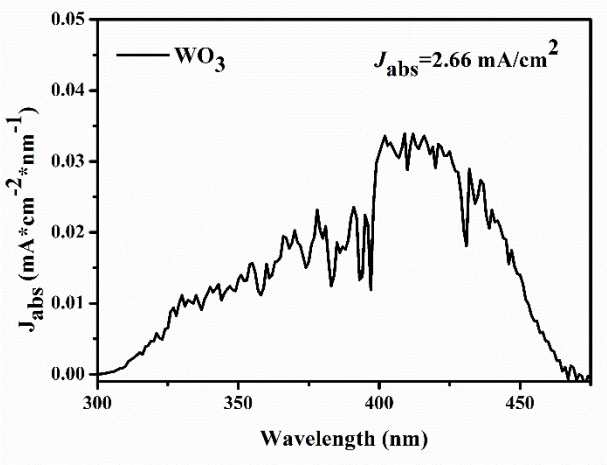

Figure S7. Photo flux and theoretical maximum photocurrent of WO_3 film.

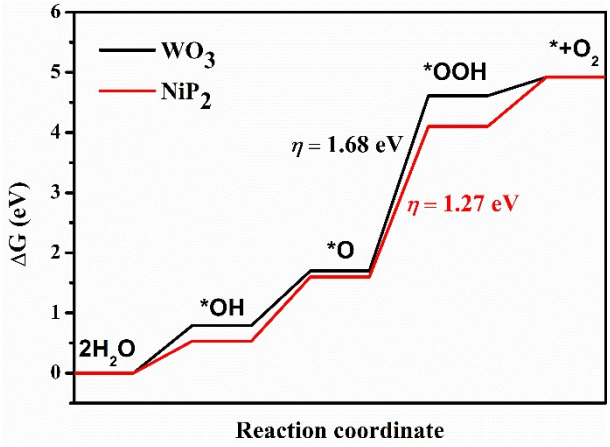

Figure S8. The Gibbs free energies and overpotentials (η) of different species adsorbed on WO_3 and NiP_2 surfaces.

Table S1 Comparison of literature with the similar catalyst system.

Photocatalyst and cocatalyst	Shift of onset potential (V)	Current at 1.23 V_{RHE} without cocatalyst (mA/cm^2)	Current at 1.23 V_{RHE} with cocatalyst (mA/cm^2)	The current enhancement at 1.23 V_{RHE}	Ref.
WO_3; NiP_x	0.25	0.35	0.89	154%	**This work**
WO_3; FeOOH	0.07	0.60	1.30	117%	[4]
WO_3; Ferrihydrite	0.06	0.34	0.61	79%	[5]
$BiVO_4/WO_3$; CoP	0.27	1.21	2.81	132%	[6]
WO_3; CoO_x	0.15	0.21	0.40	90%	[7]
ZnO/TiO_2; FeOOH	0.27	0.50	1.25	150%	[8]
Fe_2O_3; FeOOH	0.12	0.61	1.21	98%	[9]

Reference

[1] J Yang, WZ Li, J Li, DB Sun, QY Chen. Hydrothermal synthesis and photoelectrochemical properties of vertically aligned tungsten trioxide (hydrate) plate-like arrays fabricated directly on FTO substrates[J]. Journal of Materials Chemistry. 2012;22 (34):17744-17752

[2] F Zhan, J Li, W Li, Y Liu, R Xie, Y Yang, Y Li, Q Chen. In situ formation of $CuWO_4/WO_3$ heterojunction plates array films with enhanced photoelectrochemical properties[J]. International Journal Of Hydrogen Energy. 2015;40 (20):6512-6520

[3] Y Hou, F Zuo, A Dagg, P Feng. Visible light-driven alpha-Fe_2O_3 nanorod/graphene/$BiV_{1-x}Mo_xO_4$ core/shell heterojunction array for efficient photoelectrochemical water splitting[J]. Nano Letters. 2012;12 (12):6464-6473

[4] J Huang, Y Ding, X Luo, Y Feng. Solvation effect promoted formation of p–n junction between WO_3 and FeOOH: A high performance photoanode for water oxidation[J]. Journal of Catalysis. 2016;333:200-206

[5] JL Liu, ZC Shang, JX Chen, LP Wen, JK Liu. Enhanced Photoelectrochemical Water Oxidation with Ferrihydrite Decorated WO_3[J]. Catalysis Letters. 2022;152 (9):2575-2584

[6] ND Quang, PC Van, S Majumder, JR Jeong, D Kim, C Kim. Optimization of photogenerated charge transport using type-II heterojunction structure of $CoP/BiVO_4$:WO_3 for high efficient solar-driver water splitting[J]. Journal of Alloys and Compounds. 2022;899:163292-163302

[7] F Zhan, W Liu, W Li, J Li, Y Yang, Y Li, Q Chen. Efficient solar water oxidation by WO_3 plate arrays film decorated with CoO_x electrocatalyst[J]. International Journal Of Hydrogen Energy. 2016;41 (28):11925-11932

[8] Z Li, S Feng, S Liu, X Li, L Wang, W Lu. A three-dimensional interconnected hierarchical FeOOH/TiO_2/ZnO nanostructural photoanode for enhancing the performance of photoelectrochemical water oxidation[J]. Nanoscale. 2015;7 (45):19178-19183

[9] JY Kim, DH Youn, K Kang, JS Lee. Highly conformal deposition of an ultrathin FeOOH layer on a hematite nanostructure for efficient solar water splitting[J]. Angew Chem Int Ed. 2016;55 (36):10854-10858